Production, manipulation and detection of monochromatic electrons with the Timepix3

vallée Florent
M2 QLMN Nanosciences and Nanotechnologies
Year 2022/2023
Tutor : Daniel Comparat
Laboratory : Laboratoire Aimé Cotton
6 March - 13 July 2023

Production, manipulation and detection of monochromatic electrons with the Timepix3

VALLÉE Florent

M2 QLMN Nanosciences and Nanotechnologies

Year : 2022/2023

Tutor : Daniel Comparat

Laboratory : Laboratoire Aimé Cotton (LAC)

Research team : Matière Froide Corrélée

6 March - 13 July 2023

Oral defense date : 12 july 2023

Table des matières

Chapitre 1

Introduction

1.1 Presentation of the laboratory Aimé Cotton

My internship was carried out at the "Laboratoire Aimé Cotton" (LAC) with the Correleated Cold Mater (MFC) research team. The LAC is an "Unité de recherche mixte" (UMR) of the university Paris-Saclay and the CNRS. This laboratory was created on the initiative of the famous physician Aimé Cotton. The project began in 1914 and was inaugurated in july 1928.

Approximately 50 people work at the LAC. 20 researchers or research fellow, 5 PhD students, 4 emeritus. There is four teams : **Theomol, MFC, Nano3, LIDARS and Handicap** who work on different themes.

MFC works on three different scientific axis : **fundamental measures** where the themes are the control of cold molecules, the study of antimater and the measure of the electric dipole moment of the electron. The **Rydberg atoms**, with the study of Rydberg atoms of caesium or ytterbium for the developpement of quantum technologies especially quantum simulation. The **Cold electrons and ions sources** that study the developpment of ions and electrons sources based on ionization of Rydberg atoms for the developpement of spectroscopy, imaging, etc... Techniques. This last group is where I carried out my internship.

1.2 Introduction to the HREELM project

Nowadays, there are many microscopy techniques available for studying matter on a very small scale. These include for instance, optical microscopy, scanning tunneling microscopy and electron microscopy techniques. Electron microscopy methods use charged particles such as ions or electrons to observe a sample. For example, there's LEEM (Low Energy Electron Microscopy) for observing the surface with low-energy electrons (0 eV to 100 eV). There's also HREELS (High-resolution Energy Electron Loss Spectroscopy), for analyzing the energy lost by electrons to characterize and determine the chemical composition of a sample at a millimetre scale. However, we do not know any technique that will combine LEEM and HREELS allows us to resolve at he nanometric scale, the vibrational states at the surface of a sample. This is the aim of HREELM (High Resolution Energy Electron Loss Microscopy). The principle is to use low-energy monochromatic electrons and high-performance detectors to analyze the electrons after interaction with the sample. This is a collaborative project between the CEA, ISMO and the LAC. The electron source is protected by a patent, and HREELM has received European funding (ERC) to pursue its development.

1.3 Presentation of the internship

During this internship in HREELM project I worked on a number of different topics. I worked on simulations of the Stark map of the caesium atom. I also carried out diver simulations for the HREELM project to study electron trajectories in the future facility. The most important part of my work was to study Timepix3, the detector used for particle detection. The main way of doing this is through

a bibliographical study of Timepix3. I'm also trying to improve the time resolution of this sensor by combining information from several pixels. In this context, I'm working on the production of ultraviolet pulses with fourth harmonic generation. Indeed, ultraviolet pulses can be used to test the operation of Timepix3 and see if we can improve its time resolution.

Chapitre 2

The HREELM Project

HREELM uses an electron source based on the ionization of Rydberg atoms. Applying an electric field to the Rydberg atoms lifts the degeneracy of the energy levels thanks to the so called Stark effect. This gives us excellent control over electron energy, providing us with a monochromatic, low-energy electron source. In this section, I'll start with a reminder of Rydberg atoms and the Stark effect. Then I'll talk about electron trajectory modeling in HREELM and the Stark effect.

2.1 Theorie part

2.1.1 Rydberg atoms and alkali metal atoms

An atom consists of a nucleus with protons and neutrons, and an electronic shell with electrons. An electron is characterized by the quantum numbers n, l, m_l, m_s with n the principal quantum number, l the orbital angular quantum number, m_l the magnetic quantum number. Rydberg atoms are in an outgoing state and have one or more electrons with high principal number, typically $n > 10$, so that the electron can be said to be "far from the nucleus on average". Because of these properties, Rydberg atoms are larger than ground-state atoms. In the laboratory, it is possible to observe Rydberg atoms as small as $1\mu m$. The size of these atoms is directly related to the value of n thanks to the relation :

$$r = \frac{4\pi\epsilon_0 n^2 \hbar^2}{mke^2} \qquad (1)$$

With r the radius of the atom, m the electron mass and e the elementary electric charge.

Alkali metal atoms are atoms with only one valence electron. Due to this configuration, there is an analogy between the alkali metal atoms and the hydrogen atoms where the ionic core shell replace the proton. This is very usefull for the developpement of the theory of the alkali metal atoms. These atoms have very interesting properties like a long radiative lifetime proportional to n^3, or a high sensitivity to the electric field proportional to n^7. Lots of project will use these properties for the development of new technologies. There is degeneracy of the Rydberg states with the same n but for alkali this is not anymore the case due to the spin orbit coupling. The quantum defect theory gives the formula for the binding energy E(n).

$$E(n) = \frac{Ry}{(n - \delta_l)^2} \qquad (2)$$

With Ry the Rydberg constant and δ_l the value of the quantum defect. This number is roughly inversely proportional to the quantum number l. In physical terms, δ_l can be understood as the deviation of the electron's trajectory around the positively charged nucleus. When l is maximal and $\delta_l = 0$, the orbit is circular, and when l is smaller, the trajectory becomes elliptical and δ_l is larger. δ_l is a phase shift at each recursion around the nucleus due to the interaction between the electron and the ionic nucleus. When the orbit is elliptical, this phase shift is greater because the electron is closer to the nucleus, Fig 2-1.

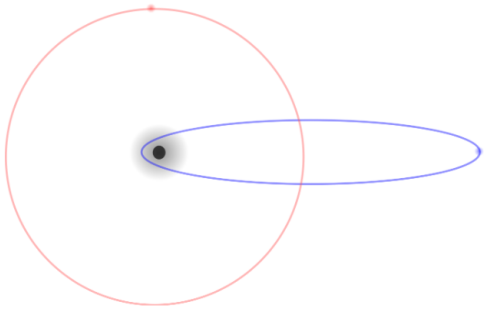

FIGURE 2.1 – Draw of the electon's trajectories. **Red trajectory :** The quantum number l is high. **Blue trajectory :** The quantum number l is low

Since Rydberg and alkali metal atoms are highly sensitive to electric fields, it's very important to understand the effect of electric fields on these atoms. Indeed, under the effect of an electric field, there is a lifting of the degeneracy of the atoms' state, known as the Stark effect. It's analogous to the Zeeman effect with the magnetic field. The electric field can lift the state degeneracy with the same n but with a different l and can also lift the state degeneracy with the same l but with a different m_l.

As we know, the Rydberg atom is in an excited state, so the electric field to ionize the atom is weaker compared to an atom in the ground state and depends on the value of n.

$$F_{ion} = \frac{5.10^{11}}{16n^4} \qquad (3)$$

2.2 The HREELM setup

HREELM is a project for electronic microscope able to technic for image the vibrational states at the surface of a sample. This project require a source of monochromatic electrons and a system of detection of the electrons. The actual version of the setup doesn't correspond at the final version of HREELM.

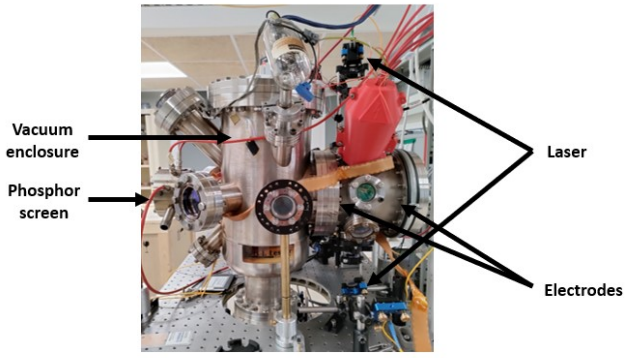

(a) Photo of the actual HREELM (HREELM 0)

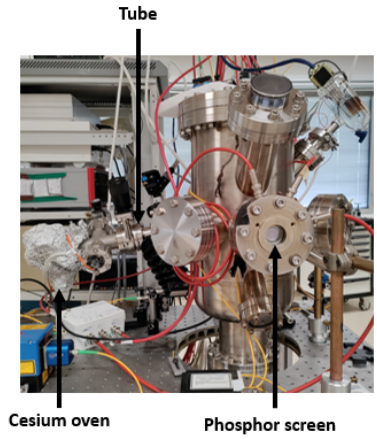

(b) Photo of the actual HREELM (HREELM 0)

In this version, only the monochromatic electron source and a simple electron detection system (phosphor screen) are used. The electron source consists of a cesium oven for emitting cesium atoms. The oven heats a liquid cesium source, and the atoms evaporate. The cesium passes through a tube and arrives at the intersection of two lasers. This tube is made of a special material to neutralize the condensation of cesium atoms in the tube. When the atoms are at the intersection of the two lasers, they are excited into a Rydberg state. There is a first transition from $6S_{1/2}$ to $6P_{3/2}$ with an 852 nm

laser, and a second transition from $6P_{3/2}$ to $7S_{1/2}$ due to a 1470 nm wavelength. A pulsed electric field applied by electrodes ionizes the Rydberg atoms and utilizes the mono-energetic electrons produced. By increasing the cesium atom flux, we can tune the electron flux. Thanks to absoprtion process of the laser by cesium atoms, we can determine this flux. After the electrons ionizations The electrons resulting from the ionization of Rydberg atoms are accelerated by electrodes so that sensors such as the phosphor screen can detect them.

In a near future (Fig 2.3), the HREELM configuration will evolve to add a sample holder. This sample holder is very special because we can change the temperature in a large domain (few kelvin to several hundred kelvin) for the chemical analyse of the matter, etc...

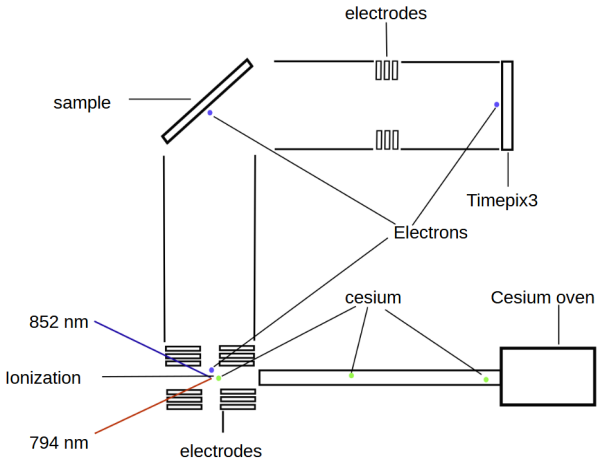

FIGURE 2.3 – Near future HREELM (HREELM 1)

There's the sample holder and the detection system for measuring electron energy as a function of time of flight. Indeed, as we use a pulse electric field, we know precisely when we ionize Rydberg atoms. By combining this information with the time of hit we can know the time of flight. This detection system consists of two microchannel plates (MCPs) with a gain of 1000 for each MCP, i.e. a total gain of 10^6. In the future, this electron flow will reach another sensor, the Timepix4, which can measure the position of each electron pulse and know when the time of hit.

One of the problem of this version is that the electron beam is not orthogonal at the sample and it's create spatial dispersion. The spatial resolution of the setup is very limited by this effect. To fix this problem, it's neccesary to modify the electrons trajectories to get a electron flux who is orthogonal to the sample. This is the reason why the final version of the HREELM will have a beam separator to modify the trajectories of the electrons. As they approach the sample, electrodes slow down the electrons so that they arrive with low energy and interact with the sample. They will then be re-accelerated in the other direction to be detected by the sensors.

2.3 Work during the internship

2.3.1 Simulation of the electron trajectories in HREELM with SIMION

The electron source based on the ionization of Rydberg atoms interacts with the sample under study to form an image of the sample's vibrational states. This image is only a few microns in size, well below the spatial resolution limit of the detectors. Indeed, an image formed on a 100 μm sample must be 10 cm in size on arrival. It is therefore necessary to magnify the image formed on the sample using electrostatic lenses. Electrostatic lenses are devices for focusing ion and electron beams by producing an electric field. Unfortunately, it's difficult to predict the effect of electrostatic lenses on electrons, so we have to simulate the electron trajectory in HREELM.

SIMION is a software package for simulating electron and ion trajectories. During my internship, I used SIMION to simulate electron trajectories in order to find the right voltages to have an exploitable

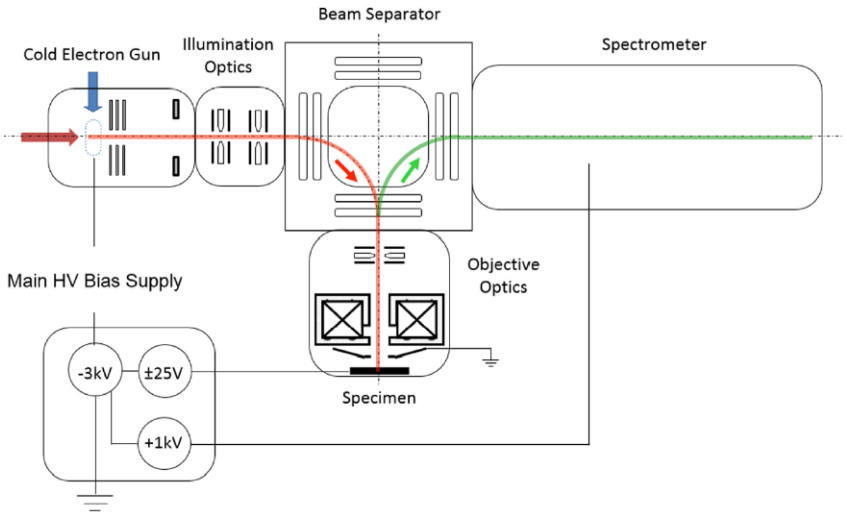

FIGURE 2.4 – HREELM final version (HREELM 2)

image of the surface sample. The initial configuration consists of a sample oriented at 45° at the entrance to a long tube. Inside this tube are 6 electrodes. Only two electrodes act as lenses, the other 4 are grounded to block the electric fields produced by the two lenses.

FIGURE 2.5 – SIMION simulation in the intial system

To begin with, I'll study a simple system, a beam of four electrons with two different initial positions and two different orientations. Two electrons are directed parallel to the tube and two others are slightly deflected. The aim is to find the right voltages to achieve a nice image of the sample, this means the electron group with the same initial position but not the same orientation should have the same final position and the distance between the two electron groups increases.

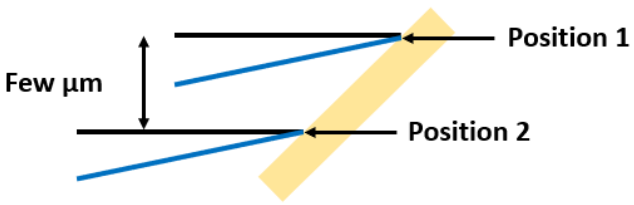

(a) Photo of the actual HREELM (HREELM 0)

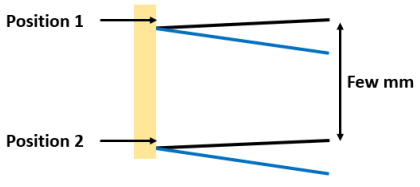

(b) Photo of the actual HREELM (HREELM 0)

To optimize the voltages, we use an algorithm in *lua* language which can optimize the electrodes voltages. The problem with the initial design was that if the electrons passed through the center of the lenses, the influence of the lenses on the electrons was negligible. So depending on the voltages we use, we have either a good resolution and a low zoom or a high zoom and a poor resolution. To increase the size of the image and keep a good resolution, electrons with a high angle of deflection had to be used at the initial position. But in this case, the voltage applied to hold the electrons in the tube is very high, so a small deviation in the position of a lens can have a major impact on electron trajectories. The

problem in the initial design was that the electrodes was far from the sample. To solve this problem, we add another lens close to the electron emission position, and choose to increase the electron deflection angle. This configuration improves zoom and resolution at the same time with low voltages.

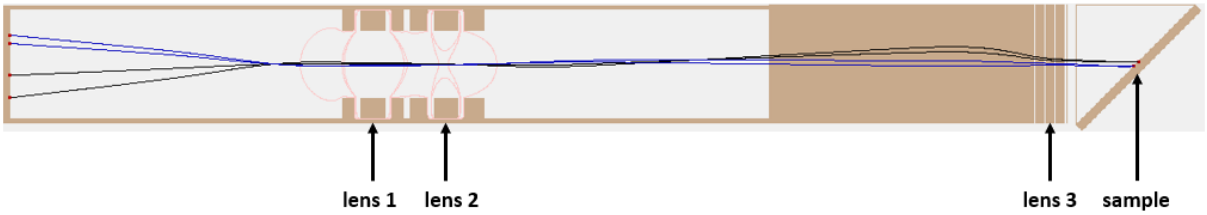

FIGURE 2.7 – SIMION simulation without faraday cage

But these lenses pose new deflection problems. They are close to the origin of the electrons (the sample), so the electric field induced by the lenses modifies the particle trajectories. This deviation in the image below, with the particles moving in an upward direction. To solve this problem, we had to protect the sample from the electric field with grille who works like a Faraday cage. Even with this cage, it's still a small deviation.

In experimental situation the image form by the interaction between incident electrons and the sample has more than 4 electrons. To be closer than this case, we increasing the number of electrons at the origin.

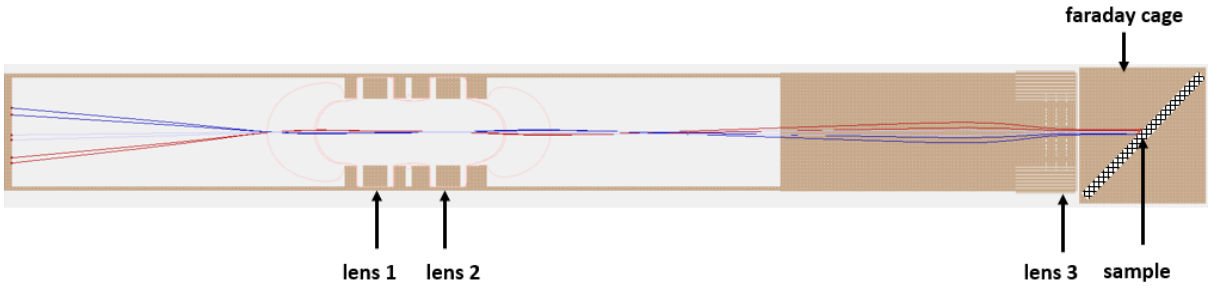

FIGURE 2.8 – SIMION simulation with a faraday cage

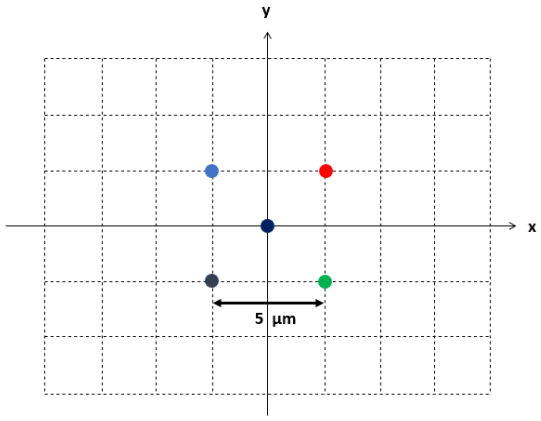

(a) Initial position of the electrons

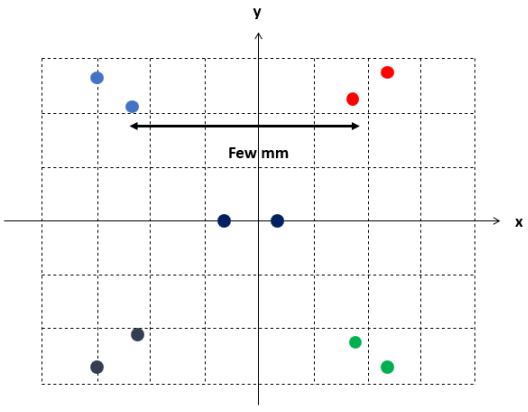

(b) Position of the electrons on the sensor

In the first image, we can see the initial positions of the electrons, i.e. the positions of the electrons on the sample. There are two electrons per point. The image size is small, but the resolution is good. The second figure shows the positions of the electrons on the sensor after the electrostatic lenses. Electrons with the same initial position do not have the same final position, and there is a deviation. This is not good because this deviation of the electrons means there is a deformation of the image. Moreover the deviation between electrons with the same initial position means that the image is defocalise.

2.3.2 Origin simulation code Robichaux

During my internship, I also carried out simulations of the Stark map of cesium atoms for different values of ionization field threshold, polarization type, etc... The simulations were carried out using the Francis Robicheaux code. Thanks to these simulations, we can see which energy levels we need to ionize and the laser wavelength required to do so.

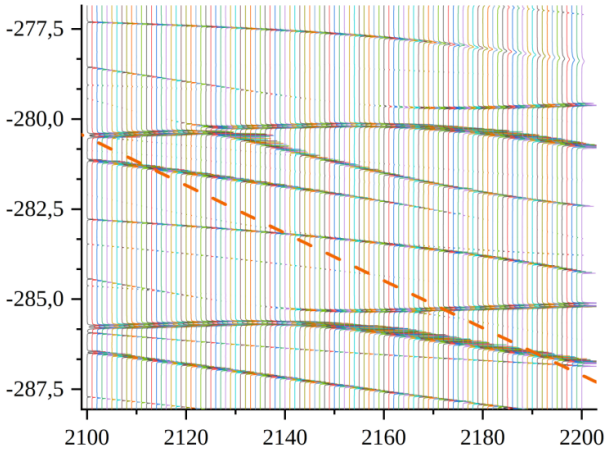

FIGURE 2.10 – Draw of the improving time resolution system

Chapitre 3

The Timepix3

3.1 Introduction

For the HREELM project, it is necessary to have very good temporal resolution and good spatial resolution with a high electron flux. Few sensors possess these three capabilities. In general, they have good spatial resolution and good temporal resolution with low flux like the delay line, or good temporal resolution and high flux but poor spatial resolution like the micro channel plate. This is why we use the Timepix3. This is a sensor developed in collaboration between CERN, Nikhef University and the University of Bonn. It has been marketed since 2013 by the Medipix collaboration. There's a more recent version of Timepix, Timepix4, which has better temporal and spatial resolution, but also better flow. This is the model that will be used for the HREELM experiment. I had to understand how Timepix3 works by reading several articles and presentations on Timepix3.

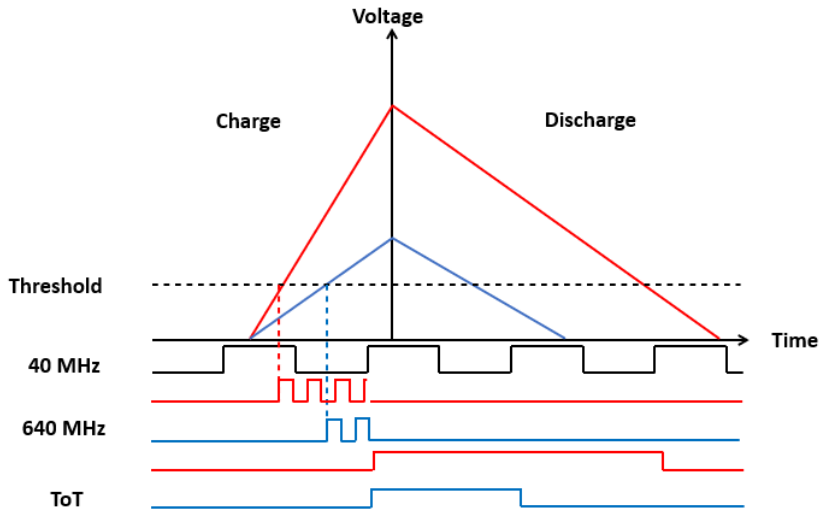

FIGURE 3.1 – Timepix3 clock structure

3.2 How the Timepix3 works

The Timepix3 is a matrix of 256x256 pixels developed in 130 nm CMOS technology, each pixel having a size of 55 μmx55 μm. The sensor can read a charge and a time. This sensor has two differents clocks, a 40 MHz clock with a time bin of 25 ns ($\frac{1}{40.10^6} = 25.10^{-9}$). This is the main clock, running continuously. There is also a 640 MHz clock with a time bin of 1.56 ns ($\frac{1}{640.10^6} = 1,56.10^{-9}$). This is a local clock specific to each superpixel. These two clocks are not synchronized. The aim of this system is to reduce power consumption and improve temporal resolution.

An electron pulse arrives at the sensor at time t_{hit}. There is a charge time during which the number of charges detected by the sensor will increase. If the total charge value exceeds the threshold (the threshold is a load limit below which the signal is not detected) before the end of the charge time, the 640 MHz clock is turned on for the superpixel within which the pixel that received the pulse is located. A superpixel is a group of eight pixels (4 rows and 2 columns) that share the same 640 MHz clock. At the rising edge of a 40 MHz bin, the 640 MHz is turn off, the number of 640 MHz bins is counted, giving the *fineToA* and the 40 MHz clock gives the *coarseToA*. With the *fineToA* and the *coarseToA* we have the *ToA (Time-of-Arrival)* thanks to the formula :

$$ToA = coarseToA - fineToA \tag{4}$$

Be careful not to confuse *ToA* and t_{hit}. Although it's called *Time-of-Arrival*, the *ToA* represents the moment when the signal "exceeds" the threshold. t_{hit} represents the moment when the signal arrives on the Timepix3.

The moment when the signal exceeds the threshold is also the begin of the *ToT* (*Time-over-Threshold*), it's the time during which the signal is always above threshold. The *ToT* uses only the 40 MHz clock. After a charge time, there is a discharge time during which the Timepix3 will lose charge. When the amount of charge has diminished to the point where we're below the threshold. Due to the 40 MHz clock bin time, the *ToT* will stop at the start of a 25 ns bin. After the end of a discharge time, a pixel needs to wait 475 ns to detect others electrons. It is important to note that discharge time depends on the discharging ratio, which is the number of charges lost for a given time. This discharge ratio is the same for each pixel. From this we can deduce that the discharging time varies proportionally with the charge incident on a pixel, and that we can therefore use the *ToT* to estimate the number of charges arriving on the pixel.

3.3 Signal discretization : *ToA* and *ToT* vs *realToA* and *realToT*

As we have already seen, *ToA* and *ToT* are values measured using 40 MHz and 640 MHz clocks. *ToA* and *ToT* are therefore discretized values. For example, the *ToA*, thanks to the *fineToA* measured with the 640 MHz clock, is incremented in steps of 1.56 ns. The *ToT* is incremented in steps of 25 ns. But the signal does not arrive at the sensor with discretization. To understand more how the Timepix3 works we assume the signal is linear. It's not absolutely true, but the approximation is reasonable. In fact, we've seen the signal curves (charge vs. time) in the electronics, and the signal is virtually linear. Due to this assumption, we can found new formulas :

$$realToA = t_{hit} + t_{rise}\frac{x_{thre}}{q} \tag{5}$$

$$realToT = \frac{q - x_{thre}}{q}(t_{rise} + r_{disch}) \tag{6}$$

realToA is the moment when the signal actually exceeds the threshold, *realToT* is the real duration during which the signal is above the threshold, q is the charge of the signal, x_{thre} is the value of the threshold, t_{rise} is the time where the charges are accumulate and r_{disch} is discharge rate.

Thanks to *realToA* and *realToT* we can recalculate *ToA* and *ToT* again.

$$ToA = (realToA \div 1,56) * 1,56 \tag{7}$$

$$ToT = (realToT \div 25) * 25 \tag{8}$$

With $\div$ the symbol for Euclidean division. This has several consequences for the measurements. Firstly, there is an uncertainty of 25 ns on the *ToT* and 1.56 ns on the *ToA*. To illustrate this, let's suppose we send an electron pulse to the sensor so that the *realToA* is equal to 12 ns, in accordance with the previous formula, the *ToA* value will be 10.92, which implies a deviation of more than 1 ns from the *realToA*. The same applies to the *ToT*. The discretization of ToA and ToT also has consequences for the threshold. Indeed, I said in the previous section that the ToT is the duration during which the signal is above the threshold, which implies that it begins when the signal exceeds the threshold and ends when

the number of loads falls below the threshold. With discretization, this is impossible : ToT starts at the beginning of the bin after the signal exceeds the threshold and stops at the beginning of the bin after the signal exceeds the threshold.

3.4 Timepix3 error source

The Timepix3 is an accurate sensor, but there are sources of error that can cause it to lose this precision. The discretization of ToA and ToT is a source of error, since it limits the resolution of Timepix3, as I explained in the previous section. But there are others source errors.

One of this source errors is due to the superpixel structure. A superpixel consists of 8 organized pixels divided into 4 lines of 2 columns. Within a superpixel, pixels share the same 640 MHz clock, thanks to the VCO. However, each pixel is not at the same distance from the VCO and does not take the same time to communicate with it. However, each pixel is not at the same distance from the VCO and does not take the same time to communicate with it. This creates an offset when an electron pulse that may exceed the threshold hits the sensor. If this pulse hits two pixels at the same time, the pixel closer to the VCO will take less time to switch on the 640 MHz clock. The signal from the second pixel will arrive a little later, giving the impression that the pulse arrived later.

There are also groups of 4 superpixels in a column, with the same 40 MHz clocks. There is an offset of 1.56 ns per double column, so after 16 double columns there is an offset of 25 ns, the duration of a bin. This is repeated every 16 double columns. So all the pixels don't have the same 40 MHz clock.

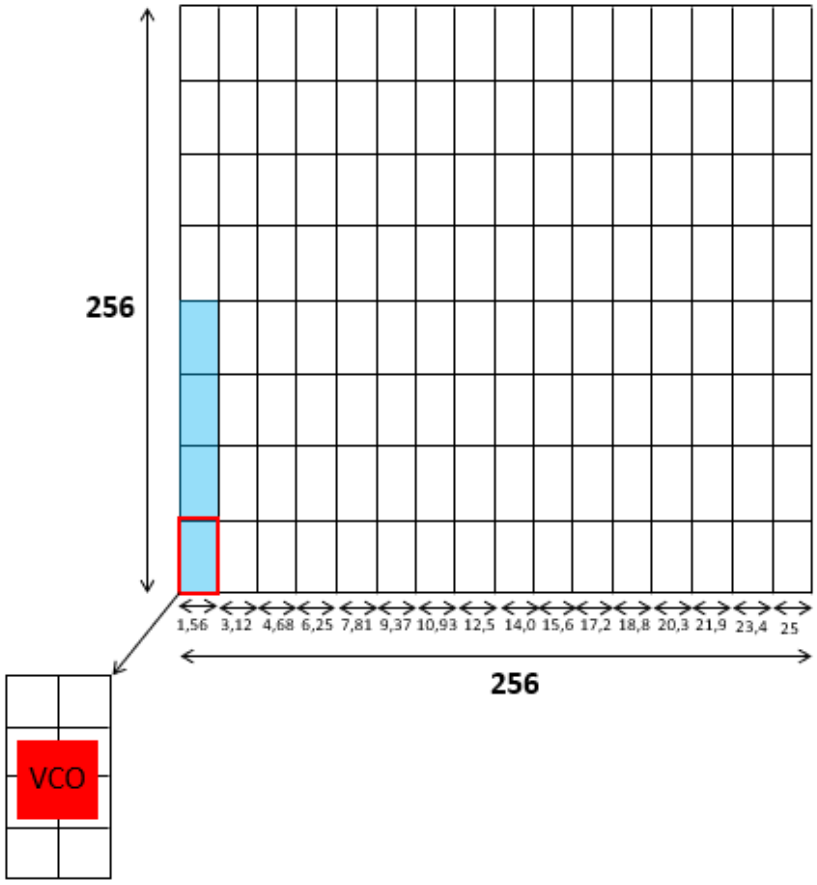

FIGURE 3.2 – Timepix3 structure with a superpixel

One of the most important error source is the timewalk. The timewalk is a temporal shift between in the pulse peak. To understand this, let's imagine we have two pulses arriving at the same time on the Timepix3, but with different intensities. As the first pulse has more electrons, it will cross the threshold

faster than the second. From the Timepix3's point of view, the first pulse arrived first. Timewalking is a major source of error. Fortunately, with careful calibration, it is possible to limit or even cancel the effects of timewalking on time resolution.

3.5 Calibration of the Timepix3

Before using Timepix3, you need to perform a calibration. Many effects, such as the timewalk, can reduce resolution, and it is therefore necessary to associate an energy value with a ToT. Various calibration techniques are available :

- **The test pulse :** it is possible in the Timepix3 hardware to inject a pulse directly in the electronic front-end circuitry of the Timepix3. We can know and choose the load we send. This is the simplest calibration technics but it's not often use because it's the same clock for the injection pulse and for the detection of the pulse, so a shift of the frequency of this clock can't be measured with this test.
- **The testbeam :** we send charged particles on the Timepix3 to characterize the detector.
- **The laser beam :** We use a laser to send photons on the Timepix3 and characterize the detector. We can use the laser beam to determine the properties of the Timepix3 with a silicon layer but also without a silicon layer due to the photoelectric effect.

All these techniques are pixel-by-pixel processes. In fact, each pixel is different from the others (not exactly the same electronics, the same capacitor, etc.) so they don't have the same threshold. This is why we use a calibration pixel-by-pixel.

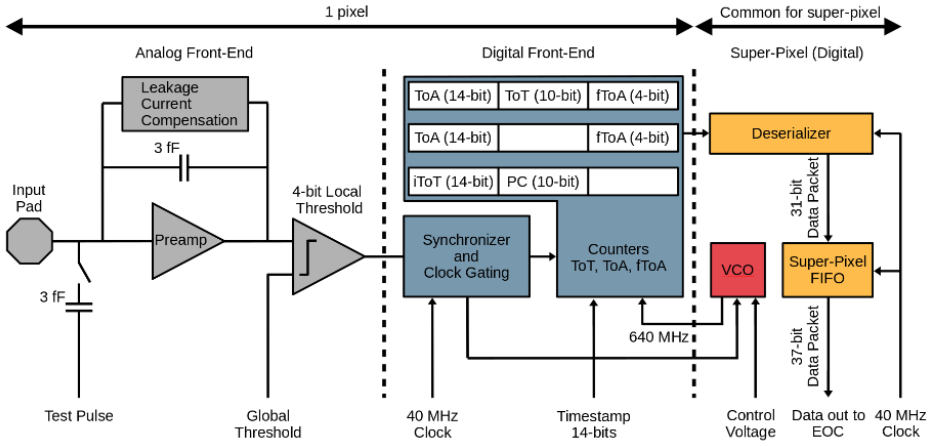

FIGURE 3.3 – Draw of the electrical components for a Timepix3 pixel

It's preferable to use an ultraviolet laser for the laser beam, as this improves photoelectric efficiency. But we don't have an ultraviolet pulse laser, so we have to make our own. To do this, we use an 820 nm femtosecond laser and double the frequency twice with non-linear crystals. The first time from 820 nm to 410 nm, the second from 410 nm to 205 nm.

For proper calibration, there are two steps. First, an energy calibration to associate a ToT with an energy value. To do this, we can perform a voltage calibration by injecting test pulses (several pulses per pixel) of different amplitudes. We record the ToT for each pulse. Next, we performed a voltage/energy calibration using different known energy sources.

The second step is time calibration. We calibrated the time march by injecting 2 pulses with a fixed delay. Next, we calibrate the delay.

3.6 Improving the time resolution

Currently, Timepix3's time bin is limited to 1.56 ns for ToA and the temporal resolution is limited at $\frac{1,56}{\sqrt{12}} = 0,45ns$. The $\sqrt{12}$ is due to the RMS calculation and the 0,45 ns value is possible with an absolute perfect calibration of the sensor, never achieve, the best time resolution is 0,62 ns. But for HREELM, we need a temporal resolution of less than 0.4 ns for t_{hit}. During my internship, I therefore tried to improve Timepix3's temporal resolution. The idea is to fix the distribution of the signal that pixels will receive initially and use information from several pixels affected by the same electron pulse to improve temporal resolution .

3.6.1 Estimation of t_{hit} with one pixel

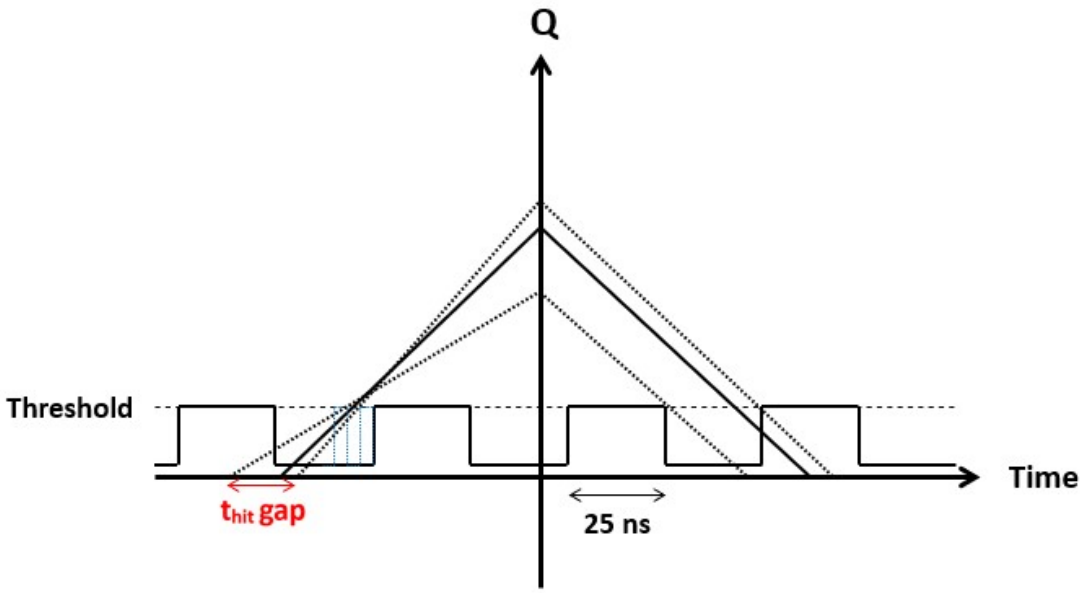

FIGURE 3.4 – t_{hit} estimate thanks to ToA and ToT

The Timepix3 gives the ToA and ToT, but not the t_{hit}, the moment when the electrons hit the Timepix3. So we need to find a way to deduce t_{hit} from ToA and ToT. Using equations (5) and (6), we can find an expression for charge as a function of $realToT$ and an expression for t_{hit} as a function of $realToA$ and charge. These expressions are not included in this document due to their complexity.

$$q_{ToT} = f(ToT) \qquad (9)$$

$$t_{hit} = g(ToA, q_{ToT}) \qquad (10)$$

One of the limitations of this method is the accuracy of ToT and ToA. Indeed, we use the time bin of ToT is 25 ns and the time bin of ToA is 1.56 ns. However, we use ToT to determine the charge q_{ToT}, so an error in the value of ToT has consequences for the value of Q. The same applies to the value of t_{hit}. In reality, there is no single value for t_{hit}, but intervals of values. The interval size represent is the precision of the t_{hit} value and depends on several parameters like the number of charges, the threshold value, etc... Some of these parameters need to be fixed, others need to be optimized.

3.6.2 Use of several pixel

By using more than one pixel, we can improve the time resolution of the Timepix3. An electron pulse is sent to a group of pixels. The t_{hit} is the same for each pixel, because the pulse arrived at the same time.

For each pixel we have a t_{hit} interval. By looking at the intersection of each interval, we can improve temporal resolution. Indeed, the true t_{hit} value is necessarily in the intersection of the t_{hit} intervals.

(a) Improvement of the t_{hit} estimation with two pixels

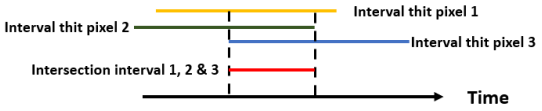

(b) Improvement of the t_{hit} estimation with three pixels

Theoritically, when we increase the number of pixel, we decrease the average time resolution. The only constraint is to fix the distribution of the signal that the pixels will receive initially. Indeed, if each pixel receives the same proportion of electrons, they have the same signal, so we don't have any more information and we can't improve the signal. For example, we take two pixels and decide that the first pixel will receive 60 % of the electrons and the second 40 %. After sending the pulse to both pixels so that the distribution between the two pixels is 60% - 40%. Each pixel has its own ToT and ToA different from the other pixel.

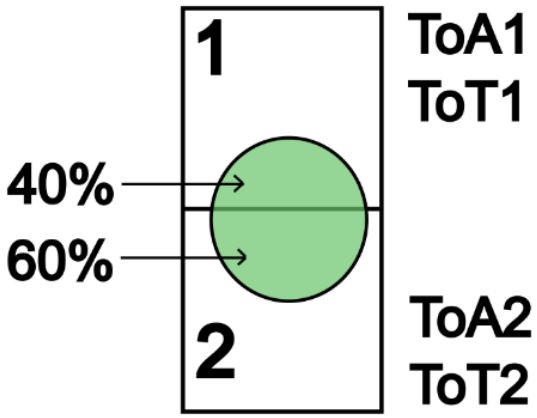

(a) Draw of the improvement dispositif

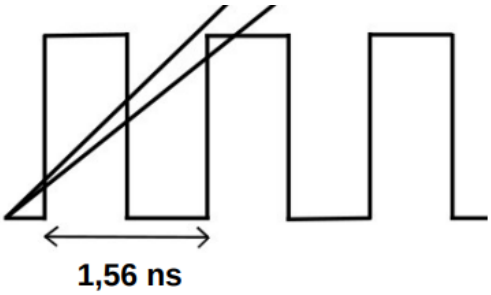

(b) Draw of the bin for the time resolution improvement

On the *Figure a*, we can see a draw of the dispositif for the time resolution improvement resolution. There are two pixels and there is a system to fix the charge distribution for each pixel. This system can be a mask like the mask for the e-beam lithography. The first pixel has 40 % and the second 60 %. A pulse is send on the two pixels and each pixel has his own ToT and his own ToA. On the *Figure b*, we can see the signal for each pixel. The pixel with 60 % crosses the threshold earlier than the pixel with 40 %. The *realToA* of the two pixels is close but due to the discretization the ToA is different with a difference of 1,56 ns for the *ToA1* and the *ToA2*.

3.6.3 Simulation of the improvement

Simulations show that it is possible to achieve a time resolution of less than 1 ns for precise values of load distribution and load number. During the simulations, we assume perfect calibration.

In this image, we see a curve of temporal resolution as a function of the number of charges and the charge distribution between two pixels. Thus, at the beginning of the axis, the first pixel has 30 % and at the end of the axis it has 50 %. The time resolution varies greatly, but we can see areas where the time resolution is less than 1 ns. These areas form a kind of valley.

From these simulations, we learn that as the number of loads increases, so does the average resolution time. When we increase the number of pixels, the average resolution time increases. This is because the amount of information on the electron pulses increases. In effect, the number of intervals for the t_{hit} increases. But the improvement depends very much on the parameters x_{thre}, t_{rise} and r_{disch}. By increasing r_{disch} we can considerably improve the temporal resolution and have a resolution of less than

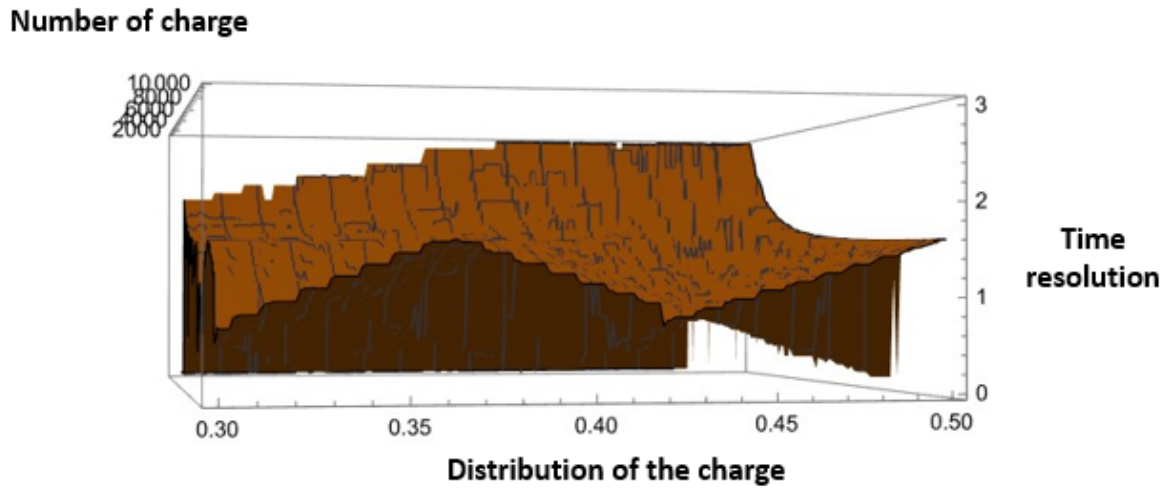

FIGURE 3.7 – Simulation for improve the time resolution

0.2 ns. This may be due to noise in the system, but this effect is not taken into account. Distribution is also a very important parameter. For a given distribution, the temporal resolution is not the same for the same number of pixels and the same number of electrons.

3.7 Second Harmonic Generation

Second harmonic generation is a nonlinear optical phenomenon in which the frequency of a beam is modified. It usually involves an interaction between the beam and a nonlinear crystal. In this phenomenon, two incident photons of the same wavelength are combined to create a new photon of a new frequency. Energy is conserved.

$$\hbar\omega 3 = \hbar\omega 2 + \hbar\omega 1 \qquad (11)$$

This phenomenon is all the more likely when the momentum is preserved :

$$\hbar\vec{k}3 = \hbar\vec{k}2 + \hbar\vec{k}1 \qquad (12)$$

Many parameters can influence SHG. We will limit ourselves to a few key parameters for SHG. To have a chance of obtaining ultraviolet light, several conditions must be met. To find the optimum conditions, we use SNLO software. SNLO is a software package for modeling nonlinear effects. All modeling work on nonlinear crystals has been carried out with SNLO.

(a) Draw of the second harmonic generation in a non linear crystal

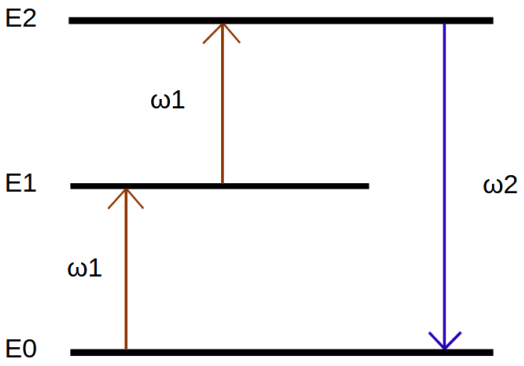

(b) Draw of the second harmonic generation with the energy level

3.7.1 Intensity of the incident beam

One of these parameters is the intensity of the incident beam. Indeed, we know from the conservation of energy equation that the maximum photon output energy is the sum of the incident photons. With SNLO, we can run simulations to observe the influence of this parameter on the output energy.

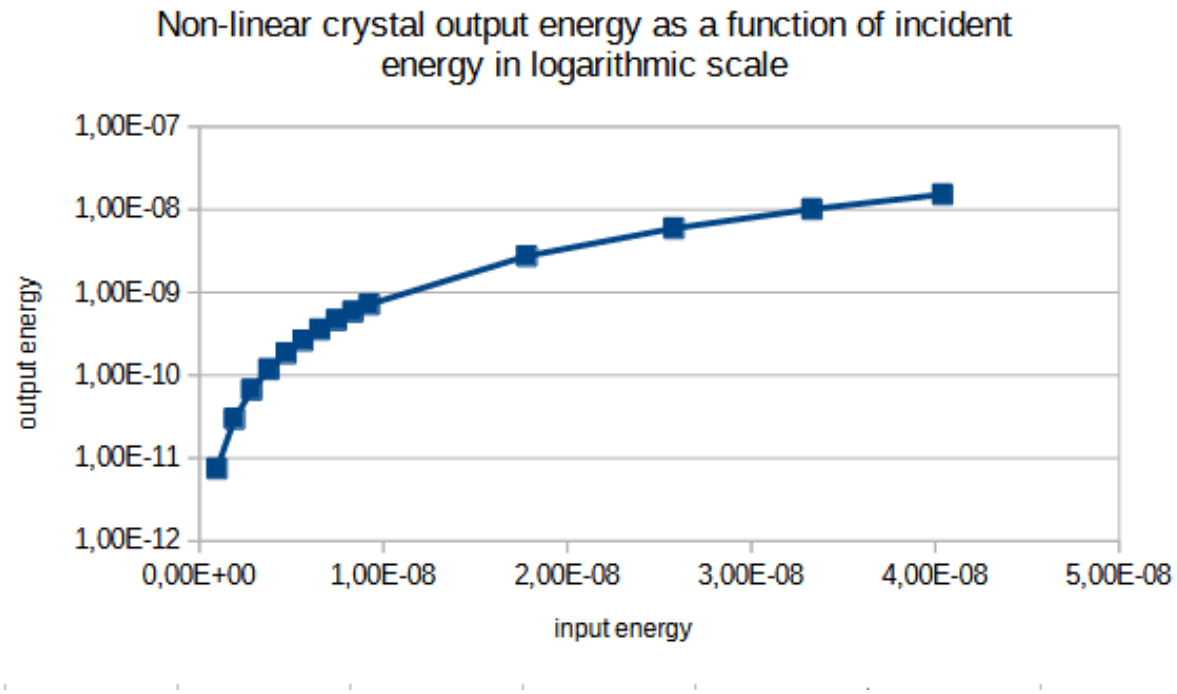

FIGURE 3.9 – Output energy for the 205 nm beam according to the input energy

The curve shows that output energy increases with input energy. The relationship between the two values is particularly strong when the incident energy is low. During my internship, I observed this effect when the laser power decreased rapidly. You can't increase the incident power in the crystal ad infinitum in order to increase the output power, as you risk breaking the crystal.

3.7.2 The phase-matching angle

The phase-matching angle is very important, because in the non-linear crystal, for a certain length, the energy of the incident beam will be converted into the new wavelength, but after this length, it's the opposite process, the energy of the SHG is converted into the initial wavelength. This is a real problem, as a variation of just a few micrometers can completely change the amount of light at the new wavelength.

$$I_2 \propto sin^2(\frac{\delta k z}{2}) \qquad (13)$$

With I_2 the second harmonic intensity, $\delta k = 2k_1 - k_2$ with k_1 the incident beam wave vector and k_2 the the second harmonic wave vector and z the propagation in the crystal.

But when the crystal is at the phase-matching angle, crystal length is irrelevant, $\delta k = 0$. This parameter has two effects for a short pulse. As the crystal length increases, so does the SHG, because the medium length increases. But pulse length and deflection also increase with crystal length.

3.7.3 Length of the non linear crystal

Crystal length is also a key parameter. Two phenomena depend on length. Firstly, when the crystal is at the phase matching angle, the gain increases with crystal length. This is because the longer the crystal is in the direction of beam propagation, the more the beam frequency can be modified. Walk-off

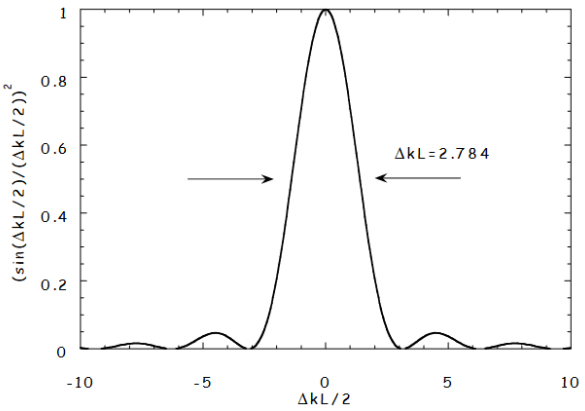

FIGURE 3.10 – Curve of the second harmonic intensity

increases with crystal length. This is because the deflection is linked to the propagation of the beam in the crystal. In the case of a pulse laser, the pulse is stretched in the crystal, and increasing crystal length increases this phenomenon.

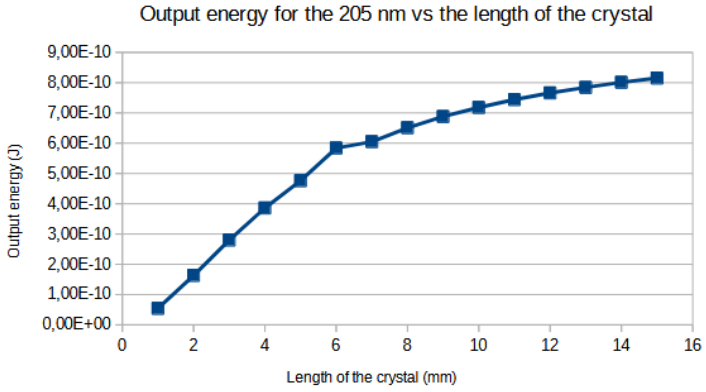

FIGURE 3.11 – Output energy for the 205 nm beam according to the BBO crystal length

3.8 Use the photoelectric effect on the Timepix3

We want use the photoelctric effect to test the Timepix3 but this effect depends on the wavelength of the beam. We can see on the picture below the curve of the photoelectric yield according to the wavelength and the material :

As wavelength decreases, photoelectric efficiency increases, so it's to our advantage to use the shortest wavelength beam possible.

As a first step, we'll check whether we can use the photoelectric effect for Timepix3. We use a pulsed laser with a repetition rate of 10 Hz. To this end, we're running an SHG from 450 nm to 225 nm. The average energy of the laser is 450 μJ. This energy level can damage the sensor, which is why we use reflection on a glass plate. We use a spherical silver mirror to focus the beam on a few pixels, but this mirror absorbs 80% of the 205 nm p-polarized beam.

We can calculate the energy sent to the Timepix3 per pulse with the calculation below :

$$Energy = \frac{0,45.10^{-3} * 0.0085 * 0.21}{10}$$

$$Energy = 78nJ$$

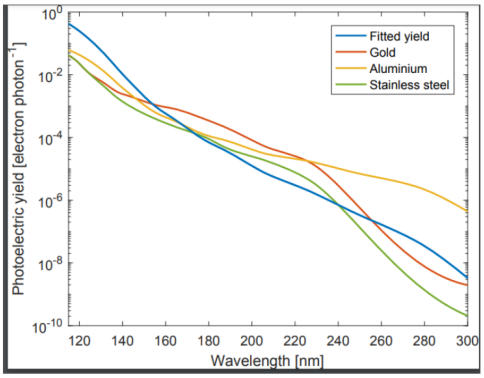

FIGURE 3.12 – Curves of the photoelectric yield according to the material and the wavelength

We sent 78 nJ on the sensor for each pulse of the laser. We can calculate the number of photons we sent on the Timepix3 with the formula below :

$$N = \frac{E\lambda}{hc} \qquad (14)$$

With N the number of photons, E the energy of the beam, λ the wavelength of the beam, h the Planck constant and c the light velocity in the vacuum. We have sent $8,8.10^{10}$ photons per pulse.

We get the figure 3.13 :

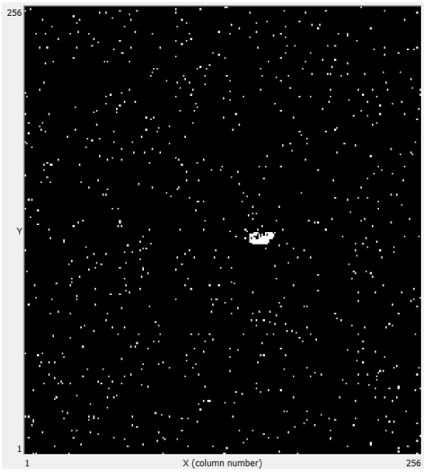

FIGURE 3.13 – Pixel matrix of the Timepix3 with the 225 nm laser beam

This image shows a representation of the pixel matrix. The white squares represent the pixels that detected a signal above threshold. Near the center, there's a white dot where we sent the laser beam. This proves that the ultraviolet laser beam creates electrons photoelectrically on the Timepix3. Unfortunately, we can't use this laser to test the Timepix3. Indeed, we need to send a pulse with a frequency of 40 MHz to synchronize with the 40 MHz clock, but the repetition rate of this laser is 10 Hz, which is too far from the Timepix3's 40 MHz frequency. We have to use another laser.

3.8.1 Generation of a short ultraviolet pulse

We use another laser, a femtosecond Ti :sapphire laser with a repetition rate of 80 MHz. We want to send a pulse for every bin of the 40 MHz clock, so we use a pulsepicker to select the pulse. The Ti :sapphire laser uses a sapphire crystal doped with titanium ions. One of the advantages of these lasers is their wavelength variability. The Ti :sapphire we use can emit from 690 nm to 1060 nm. Unfortunately, this type of laser cannot emit UV, so we have to use a non-linear crystal.

Materials :

— Laser femtosecond Ti :saphirre Mai Tai
— Pulsepicker Spectra Physics
— 1 mm BBO crystal thickness 820 nm - 410 nm
— 12 mm BBO crystal thickness 410 nm - 205 nm
— Set of lenses with different focales
— Quartz prism
— Grating

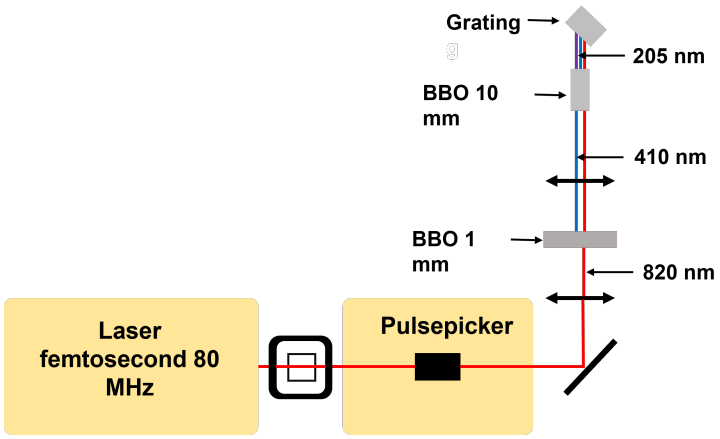

FIGURE 3.14 – Experimental setup of the fourth harmonic generation

We use 820 nm, and at this wavelength, the power is 2.5 W. The laser passes through a glass $\frac{lambda}{2}$ and into a glass cube that changes polarity. We sent the laser into the pulsepicker. The pulsepicker consists of two converging lenses and an acousto-optic crystal. The propagation of acoustic waves at a specific frequency induces a variation in refractive index. This phenomenon creates interference and enables the pulse to be selected.

At the end of the pulse collector, the 820 nm are focused in a 1 mm BBO crystal to convert them to 410 nm. A second lens focuses the 410 nm into another 12 mm BBO crystal, converting the 410 nm into 205 nm. The lenses are very important, as high intensities are required to generate a second harmonic. But we can't increase laser power, so the solution is to reduce beam size by focusing.

The laser beam contains all three wavelengths, but we want to keep only the 205 nm wavelength. Using a quartz grating or prism, we can separate the 205 nm from the other wavelengths and at the same time verify the presence of the 205 nm. The ultraviolet beam can be seen using fluorescent paper. However, as blue scattering is very strong, it is difficult to tell the difference between 410 nm and 205 nm. As glass absorbs the 205 nm wavelength, we use a glass plate to check for DUV.

For the SHG, others setup have been tested, the goal is to have the more collimated beam as possible and the smallest waist as possible. We have tested setup with a telescope for the SHG or sytem with one lense before the 1 mm BBO crystal.

After sending the ultraviolet to the Timepix3, it unfortunately fails to detect the UV pulse. This is probably due to the fact that the UV pulse has very low energy and the number of photons is very low. Indeed, with the previous laser, the number of photons per pulse was estimated at $8.8.10^{10}$, representing an energy of 78 nJ. With the Mai Tai laser, there is an energy of 30 nJ per pulse for the 820 nm beam, i.e. $1.35.10^{11}$ photons per pulse. But there's a loss with SHG. After the first SHG, 90% of the power is lost. Since it's difficult to measure DUV, we don't have an estimate of the UV pulse, but we can imagine that losses are greater than 90%.

To solve this problem, we use a more powerful laser. This is a pulse-amplified femtosecond laser. The repetition rate is 4 kHz and the average energy is 1 mJ. But the wavelength of this laser is 800 nm. This means that we make a first SHG from 800 nm to 400 nm and a second SHG from 400 nm to 200 nm. But we don't observe the presence of 200 nm after the FHG. After several trials and investigations, we understand that BBO crystals cannot produce a 200 nm beam per SHG. In fact, BBO has a broad phase-matchable range from 409.6 to 3500 nm.

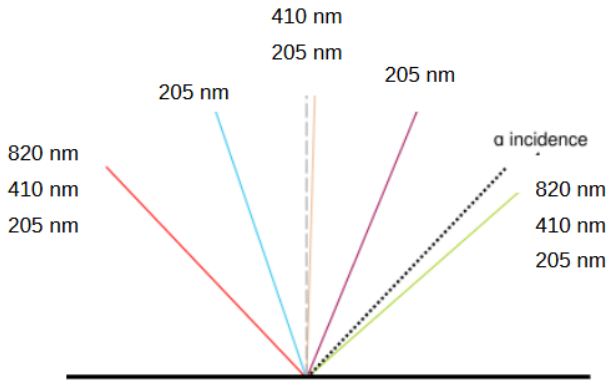

FIGURE 3.15 – Grating distribution

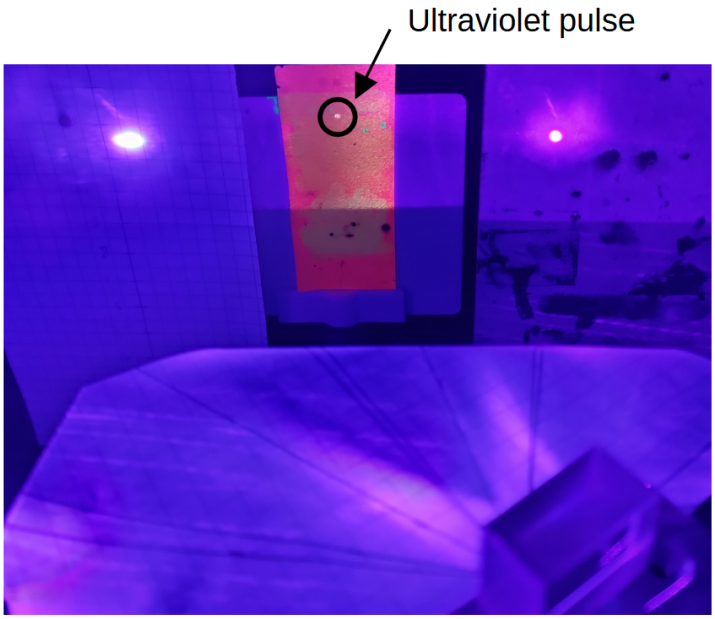

FIGURE 3.16 – Ultraviolet pulse on fluorescent paper

There are two possibilities for producing 200 nm. Firstly, we use a different type of non-linear crystal to achieve SHG from 400 nm to 200 nm. Secondly, we use a different process from SHG to achieve 200 nm with BBO. For the first idea, we want to use a KBBF crystal, which is the only crystal that can achieve SHG at 400 nm. For the second idea, we want to mix the frequencies of 800 nm and 266 nm to obtain 200 nm in a BBO crystal. The 266 nm is produced by mixing 800 nm and 400 nm in a BBO crystal. We don't have test these technique for the moment but we hope to be able to test them soon.

Conclusion

During my internship at the laboratory Aimé Cotton, I worked on the HREELM project on different subjects. I studied a mono-energetic electron source derived from the ionization of Rydberg atoms. I simulated my electron trajectory in the HREELM device to find the right configuration to obtain a good image of the sample. I also simulated the Stark map thanks to the Francis Robichaux's code. One of the most important parts of my internship is the study of Timepix3, a sensor that will detect electrons interacting with the sample. I also tried to improve the temporal resolution of this sensor by combining information from several pixels. To test this method I produced picosecond pulses of ultraviolet light using the second harmonic generation. During this internship, I familiarized myself with SIMION software for simulating electron trajectories. I also learned about nonlinear crystals for ultraviolet production. Doing this internship at the Aimé Cotton laboratory was very rewarding.

Acknowledgements

I would like to thank Daniel Comparat for accepting me as an intern, for helping me throughout the internship and for allowing me to apply for a PhD on the HREELM project. I would also like to thank the Aimé Cotton laboratory for its warm welcome. I would particularly like to thank Hans Lignier for allowing me to use a 225 nm laser to test the photoelectric effect. I would also like to thank François Nez of the Kastler Brossel laboratory for lending us BBO crystals and for his advice on SHG. I would also like to thank Elsa Cassette from Lumin for welcoming us to her laboratory and allowing us to use her 1 mJ pulsed laser.

Bibliography

— [1] D.Comparat, ERC Advanced Grant 2021 Research proposal [Part B1] Correlated Ion elecTRon fOr Nanoscience CITRON (2021)

— [2] R.Hahn , Ionisation of caesium Rydberg atoms for a mono-chromatic electron source for applications in electron microscopy and spectroscopy (2021)

— [3] R.Geertsema, Dialing back time on Timepix3 A study on the timing performance of Timepix3 (2019)

— [4] T.Dreier, Design and Verification of a USB 3.0 Readout System for Timepix3 Hybrid Pixel Detectors (2018)

— [5] F.Pitters, N. Alipour Tehrani, D. Dannheim, Time and Energy Calibration of Timepix3 Assemblies with Thin Silicon Sensors (2018)

— [6] F.Pitters, N. Alipour Tehrani, D. Dannheim, Time resolution studies of Timepix3 assemblies with thin silicon pixel sensors *JINST* (2019)

— [7] M.De Gaspari, J.Alozy, R.Ballabriga Design of the analog front-end for the Timepix3 and Smallpix hybrid pixel detectors in 130 nm CMOS technology *JINST* (2013)

— [8] Tuomas Poikela Architecture for Hybrid Pixel Readout Chips (2015)

— [9] C.Brezinaa, Y.Fua, M.De Gaspari The Timepix3 chip *ESE Seminar* (2014)

— [10] J.Jakubek Precise energy calibration of pixel detector working in time-over-threshold mode *Photoniques 116* (2011)

— [11] X. Llopart, R. Ballabriga, M. Campbell Timepix, a 65k programmable pixel readout chip for arrival time, energy, and/or photon counting measurements *Nuclear Instruments and Methods in Physics Research A 581 (2007)*

— [12] M.De Gaspari Design of the analog front-end for the Timepix3 and Smallpix hybrid pixel detectors in 130nm CMOS technology *TWEPP 2013, Perugia*

— [13] R.Jiang, D.Mou, Y.Wu, VUV laser based spectrometer for Angle Resolved Photoemission Spectroscopy (ARPES) (2022)

— [14] P.Segonds, B.Boulanger, P.Schunemann Nonlinear crystals for frequency conver-

sion *Nuclear Instruments and Methods in Physics Research A 633* (2022)

— [15] J. Faure, J. Mauchain, E. Papalazarou Full characterization and optimization of a femtosecond ultraviolet laser source for time and angle-resolved photoemission on solid surfaces *Rev. Sci. Instrum. 83, 043109* (2012)

— [16] L.Kang, Z.Lin Deep-ultraviolet nonlinear optical crystals : concept development and materials discovery *Light : Science and Applications* (2022)

— [16] L.Kang, Z.Lin Deep-ultraviolet nonlinear optical crystals : concept development and materials discovery *Light : Science and Applications* (2022)

— [17] P.Susnjar, A.Demidovich, G.Kurd A novel common-path scheme for fourth harmonic generation by ultrashort laser pulses *Optics Communications 528 129031* (2023)